Test-Bed for evaluation of impact of evil waveforms on real receivers and SQM performance

Christophe Macabiau, Willy Vigneau, Dominique Houzet

Test-Bed for Evaluation of Impact of Evil Waveforms on Real Receivers and SQM Performance

Christophe MACABIAU, *ENAC*
Willy VIGNEAU, *M3SYSTEMS*
Dominique HOUZET, *INSA Rennes*

BIOGRAPHY

Christophe Macabiau graduated as an electronics engineer in 1992 from the ENAC (Ecole Nationale de l'Aviation Civile) in Toulouse, France. Since 1994, he has been working on the application of satellite navigation techniques to civil aviation. He received his Ph.D. in 1997 and has been in charge of the signal processing lab of the ENAC since 2000.

Willy Vigneau graduated as a telecommunications engineer from SupAéro (Ecole Nationale Supérieure de l'Aéronautique et de l'Espace) in Toulouse, France. Since 2000, he has been responsible of the radionavigation unit at M3Systems (signal processing applied to radionavigation, applications of satellite navigation).

ABSTRACT

Several types of failures can occur in the GPS satellites that transmit the ranging signals to the users. Among them, a specific type of failure in the signal generation process aboard the satellite may result in an anomalous waveform being transmitted, called an 'evil waveform'. Evil waveforms are GPS signals that have a distorted PRN code modulation waveform. The main impact is a rupture of the symmetry of the cross-correlation peak inside the tracking channel, therefore inducing a different measurement error for two receivers that would not have the same architecture. As a consequence, there is a potential for evil waveforms to induce large tracking errors of differential systems if left undetected.

Simulations of the impact of these evil waveforms using simplified GPS receiver simulators with harmonized assumptions have been conducted by several teams. This includes simulations of the performance of the ground monitoring techniques (SQM) and tracking errors induced by these waveforms. In addition, several studies were carried out to analyze the behavior of real receivers tracking evil waveform signals among which is the reported study.

Indeed, a joint M3S/ENAC team has developed for ESTEC a test-bed to increase the knowledge on the true effect of evil waveforms on real receivers. The test set-up enables to feed real receivers with GPS signals affected with any evil waveform in the threat model.

The aim of the proposed paper is to report the measured impact of evil waveform on real receivers and to compare it with simulation results, as well as to present an assessment of the real performance of one Signal Quality Monitoring technique.

The paper starts with a brief overview of the threat model and existing studies on the subject. Next, we present the test bed architecture that has been developed: overall architecture, baseband generation board, modulation, off-the-shelf receiver. Then, we present the observed correlation functions as well as the observed tracking error induced by evil waveforms and compare them with the predicted correlation shapes and tracking errors. Then, we present the observed SQM performance in presence of evil waveforms and compare it with its predicted performance. Finally, we present an assessment of the SQM false alarm performance on live signals.

I. INTRODUCTION

Evil waveforms are GPS signals that have a distorted PRN code modulation waveform. The deformation is modeled by a lead or a lag of the rising or falling edges of the modulation code, and/or by a second-order filtering of this waveform.

The main impact is a rupture of the symmetry of the cross-correlation peak inside the tracking channel, therefore inducing a different measurement error for two receivers that would not have the same architecture.

As a consequence, there is a potential for evil waveforms to induce large tracking errors of differential systems. This potential danger pushed the Global Navigation Satellite System Panel (GNSSP) of the International Civil Aviation Organization (ICAO), and the RTCA SC-159, to propose sections in the standards that would guarantee the safe operation of differential GPS.

Several teams gathered their efforts to tackle that problem, and it was proven from simulation results that an adequate ground monitoring technique exists and that constraints on the airborne receiver could be proposed to

make sure the differential tracking error does not exceed the required accuracy level.

Simulations of the impact of these evil waveforms using simplified GPS receiver simulators with harmonized assumptions have been conducted by several teams. This includes simulations of the performance of the ground monitoring techniques and tracking errors induced by these waveforms [Macabiau and Chatre, 2000], [Phelts et al., 2000]. In addition, several studies were carried out to analyze the behavior of real receivers tracking evil waveform signals [Macabiau and Chatre, 2000], [Mitelman et al., 2000], [Phelts et al., 2000], among which is the reported study [Macabiau et al., 2001].

ESTEC has decided to develop a test-bed to increase the knowledge on the true effect of evil waveforms on real receivers since few results existed on the subject at the time the project was launched. The test set-up allows to :

- understand how real receivers behave when tracking evil signals (deformation of correlation function, acquisition and tracking points),
- find-out if their behavior is conform to what can be predicted using receiver simulators,
- analyze what exactly is the performance of the different ground monitoring techniques.

This test-bed is developed jointly by M3SYSTEMS, ENAC and Dominique Houzet.

II. EVIL WAVEFORM MODEL

The evil waveform is a GPS signal that has a distorted PRN code modulation waveform. The failure giving birth to an evil waveform occurs in the code modulation generation channel only, therefore the transmitted carrier is not affected. Two types of failure can occur that result in an evil waveform being radiated. A failure in the digital code chip generation module can alter the synchronization of some of the C/A code chip edges. A mismatch of the analog band-limiting filter can distort the physical waveform being transmitted.

As a consequence, the model proposed in [Enge et al., 1999] is a PRN signal affected by one or both of the following effects:

1. All the falling edges or all the rising edges of the code modulation are delayed or advanced by an amount of Δ seconds. If there is a lag, then Δ is positive, if there is a lead, Δ is negative. Δ is usually expressed in chips, as a multiple of the chip length T_c=1/1.023·10^6 s.
2. The modulation is filtered by a 2nd order filter characterized by two parameters:
   - $\sigma=\delta\omega_n$ where δ is the damping factor and $\omega_n/2\pi$ is the frequency.
   - $F_d = \frac{\omega_n}{2\pi}\sqrt{1-\delta^2}$ is the resonant frequency.

   Usually, σ and F_d are expressed in MHz.

Several types of threat models are considered:

- Threat model A: this type of evil waveform contains only the lead/lag effect. In that case, σ=0, F_d=0 and the accepted range of values for Δ is: –0.12 $T_c \le \Delta \le$ 0.12 T_c.
- Threat model B: this type of evil waveform contains only the 2nd order filtering effect. Therefore, Δ=0 and the possible range of values for σ and F_d is: 0.8 *MHz* $\le \sigma \le$ 8.8 *MHz*, 4 *MHz* $\le F_d \le$ 17 *MHz*.
- Threat model C: this type of evil waveform contains both effects. The possible range of values is: –0.12 $T_c \le \Delta \le$ 0.12 T_c, 0.8 *MHz* $\le \sigma \le$ 8.8 *MHz*, 7.3 *MHz* $\le F_d \le$ 13 *MHz*.

III. IMPACT OF EVIL WAVEFORM ON RECEIVERS

It can be shown that the magnitude of the error induced by a model A evil waveform only depends on the magnitude of Δ and not on its sign. Therefore, in the following, we will only consider positive values of Δ.

The effect of a model A evil waveform on the baseband transmitted signal power spectrum density is presented in figure 1 for $\Delta=0.12\ T_c$. As we can see on this figure, the effect of a model A EWF is twofold:

- A line spectrum is added to the original C/A code spectrum. This line spectrum is composed of lines placed at each multiple of F_c=1.023 MHz. The weight of these lines has a $\sin(\pi f\Delta)/\pi f\Delta$ envelope that has its 1st zero at the frequency $1/\Delta$ Hz.
- The power of the $\sin(\pi f F_c)/\pi f F_c$ envelope of the original C/A code line spectrum is severely reduced when the $\sin(\pi f\Delta)/\pi f\Delta$ envelope reaches its maximum.

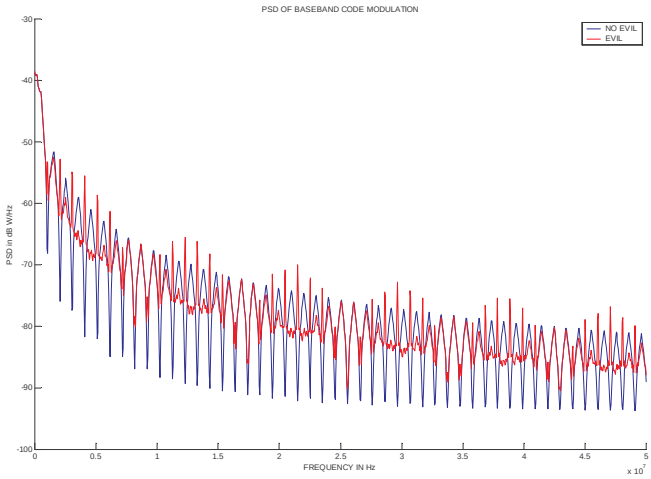

Figure 1 : *Baseband GPS signal Power Spectrum Density (Fd=17 MHz).*

The presence of the lead/lag effect mainly introduces a plateau at the top of the C/A code correlation function and shifts that function by $\Delta/2$. Inside the tracking channel, the plateau is more or less rounded, depending on

the IF filter transfer function. The resulting tracking error will then depend on the DLL discriminator function. For example, if the DLL is an E-L loop, if the chip spacing is larger than Δ, then the error is close to $\Delta/2$. If it is lower, then the tracking point is inside the rounded plateau.

As shown in figure 2, model B evil waveforms raise all the frequency components of the code spectrum located around F_d,. As a result, the cross-correlation function is also filtered by the 2nd order filter.

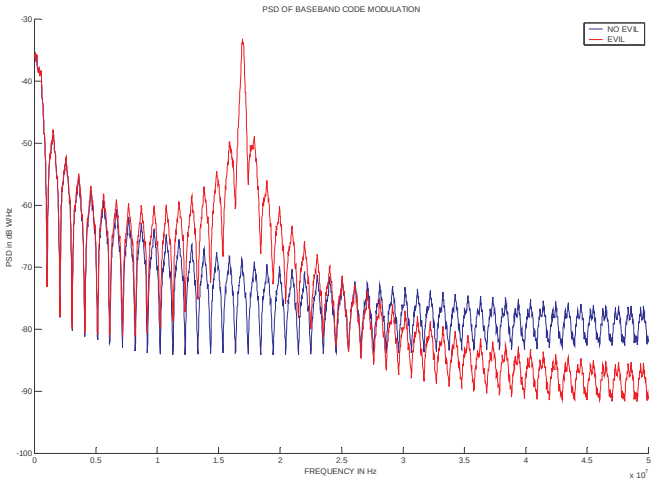

Figure 2 : *Baseband GPS signal Power Spectrum Density (Fd=17 MHz).*

Inside the tracking channel, that modification of the signal spectrum may not be perceptible if the single sided bandwidth of the IF filter receiver is lower than *Fd*. In that case, the induced tracking error is close to zero. In the other case, the correlation function inside the DLL is filtered by the 2nd order filter and therefore presents ripples. Depending on the DLL discrimination function, these ripples shift the tracking point and can even induce false locks as the correlation function presents local maxima.

Model C evil waveforms are a combination of the lead/lag effect with the 2nd order filtering effect.

The effect of a model C evil waveform is a combination of model A and model B effects. Note however that for a model C, *Fd* has a reduced range.

IV. TEST-BED ARCHITECTURE

The general test bed architecture can be broken down into the following building blocks :

- Baseband IF Signal generator**:** This generator is designed to output the baseband evil waveform signal. It includes a digital unit providing analog undisturbed baseband GPS signals with two different C/A codes (PRN1 and PRN2) . One of these signals goes through a module that provides the lead/lag effect on the rising edge of chips, the output is the model A evil waveform. This signal is then fed to a 2nd order filter designed to add model B evil waveform generation capability. The output of this baseband IF signal generator is the sum of the undisturbed signal and the model A, B or C evil waveform, both in baseband. The whole signal generator functions are provided by a numeric card (FPGA) described in Section V.
- RF Signal generator**:**. This is an Off The Shelf signal generator performing the modulation of the L1 carrier by the baseband modulation signal. The selected equipment is vector signal generator – SMIQ – Rohde & Schwarz.
- Receiver: For determining the measurement error induced by evil waveforms, the receiver can be any GPS receiver providing raw data output. For testing the performance of evil waveform monitoring techniques, the receiver selected is a NovAtel Millenium receiver with specific multi-correlator software (Cf. Section VI). This receiver will also be extensively used for range error analysis due to its large RF bandwidth and its capability to have various chip spacings and discriminator types.
- Evil waveform events monitoring: The system is composed of the NovAtel Millenium receiver with the multi-correlator software, whose outputs are collected in real time with a LabView module running on a PC, implementing an SQM technique.

The Test Bed architecture is illustrated in figure 3:

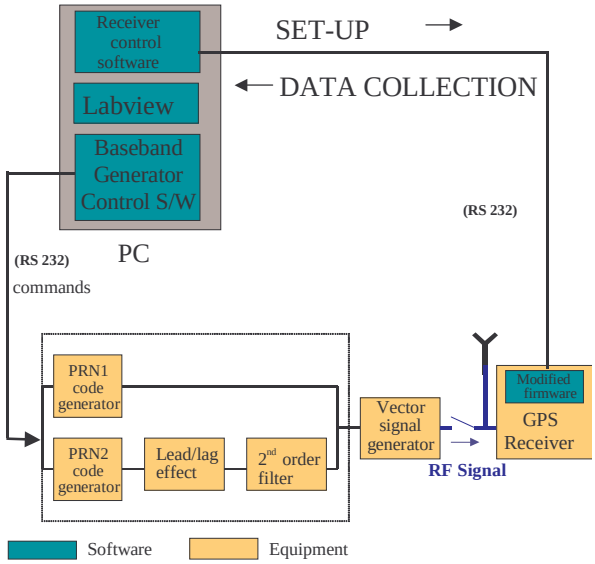

Figure 3: *Test Bed Configuration.*

Figure 4 shows a picture of the test bed that has been developed. The baseband signal generator block is provided by the electronic card – metallic box-, the RF signal generator is the SMIQ 02B at the bottom-left of the picture, events monitoring is achieved by the computer, and the receiver is the black box on the generator. The additional equipment used for development and validation phases is a frequency meter and an oscilloscope (on the SMIQ).

Figure 4: Picture of *evil waveform Test Bed.*

V. EVIL WAVEFORM GENERATOR

The baseband generator board is using a set of a digital unit delivering model A evil waveforms, and the 2nd order filter. The digital unit is designed to output the analog baseband GPS signal including rising or falling edge shifts corresponding to model A evil waveforms. This unit is a FPGA circuit reading memories containing valid navigation messages and the PRN to be generated. The FPGA also has the capability to delay the rising or the falling edges of the bit transitions by triggering counters driving latches.

This output is then fed to a 2nd order filter implemented in the second digital unit. The combination of the module adding the delays on the bit transitions and the 2nd order filter allows the generation of any GPS evil waveform.

Two PRNs signals are generated in baseband: one of them is not affected by the evil waveform, the second one is affected. This is done so that the GPS receiver can provide two pseudorange measurements than can be differenced to yield directly the pseudorange measurement error induced by the evil waveform.

The entire generator needs to be tied to a common clock. That common clock is the 10 MHz reference synchronization signal that is output by the SMIQ OCXO. The FPGA board uses that 10 MHz reference signal to trigger the generation of the C/A code chip edges. That 10 MHz reference is also internally used by the SMIQ itself to generate the L1 carrier. Such synchronization is required so that the receiver can track signals for which the dynamics on the carrier is identical to the dynamics on the code modulation.

The general architecture of the board used to generate the evil waveform is given in figure 5:

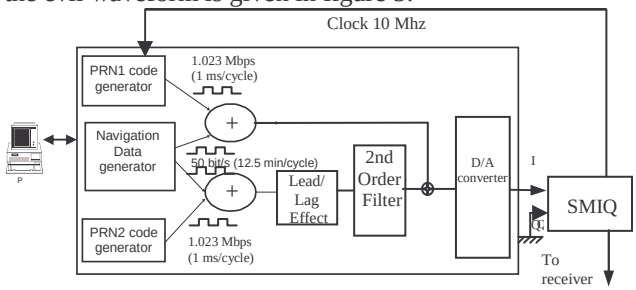

Figure 5: *Evil waveform generator architecture.*

The level of synchronization achieved and the fact that we are using a complete navigation message that is repeated gives a high quality signal that can be tracked by the receiver for hours. As an example, figure 6 shows the code tracking error that can be observed with a nominal signal when no evil waveform is applied.

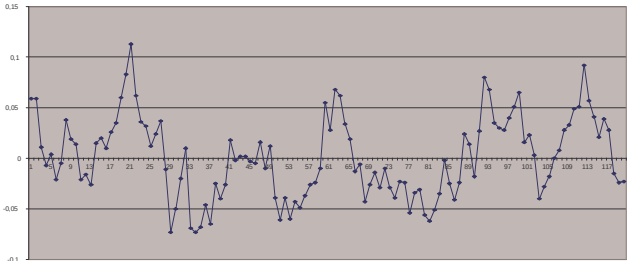

Figure 6: *Nominal tracking error in absence of evil waveform.*

As we can see, the error is centered and the standard deviation is lower than 5 cm.

VI. MULTICORRELATOR RECEIVER

The receiver used in the test-bed is a Novatel Millenium receiver. That receiver can provide as much as 48 correlator output pairs (48 on I, 48 on Q), where all correlators are slaved to the punctual determined by one tracking pair in one tracking channel. The configuration of the tracking channel is determined by the firmware.

The first firmware has a single tracking channel providing 48 correlator output pairs with 5 distributions (evenly spaced correlator, leading or trailing edge only, peak intensive distribution, and ultra wide spacings). Correlator ouputs observed with the first configuration with nominal signal conditions are shown in figure 7.

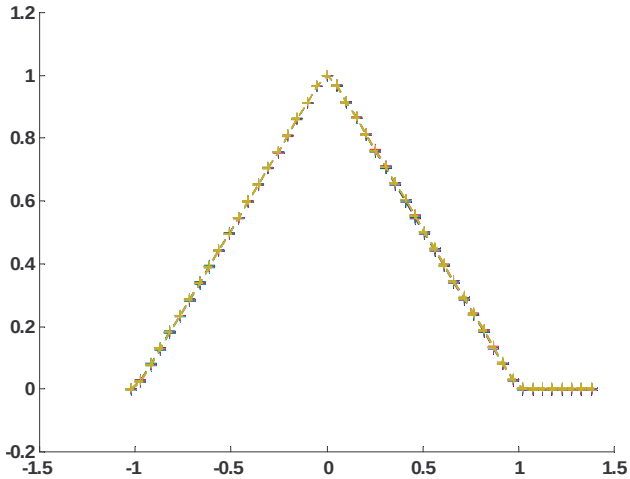

Figure 7: *Nominal correlator outputs with the 1st firmware configuration.*

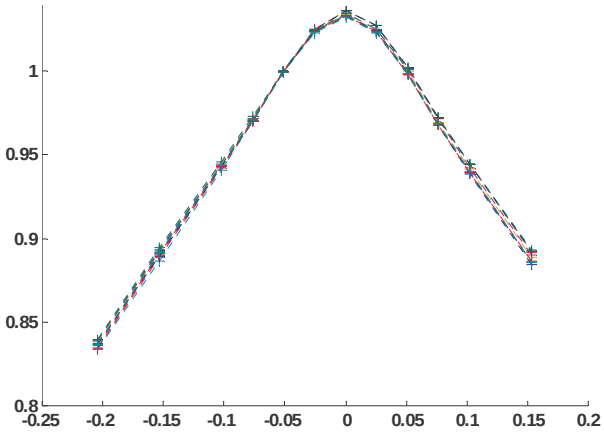

Figure 8: L*ocation of the 12 correlators w.r.t prompt in the 2nd firmware version (designed for SQM implementation).*

The second firmware is a multiple correlator delivering 12 correlator pair values (12 I and 12 Q) for 4 tracking channels. In each channel, all the correlators are slaved to the tracking pair and placed at the location (in each of the 4 channels) as illustrated in figure 8. This software version is designed to implement the SQM candidate 2b described in [Macabiau and Chatre, 2000].

Finally, the third firmware version has a single tracking channel and allows 4 chip spacings (0.05, 0.1, 0.2, 0.5, 1.0) with traditional dot-product discriminator (figure 7), and 3 chip spacing sets (0.05-0.1, 0.1-0.2, 0.2-0.4) with double delta discriminator, as shown in figures 9 and 10.

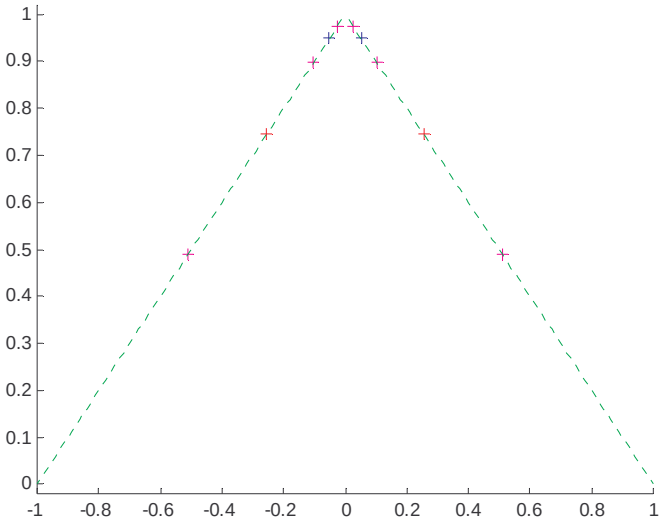

Figure 9: *Possible E-L tracking pairs with 3rd SW version.*

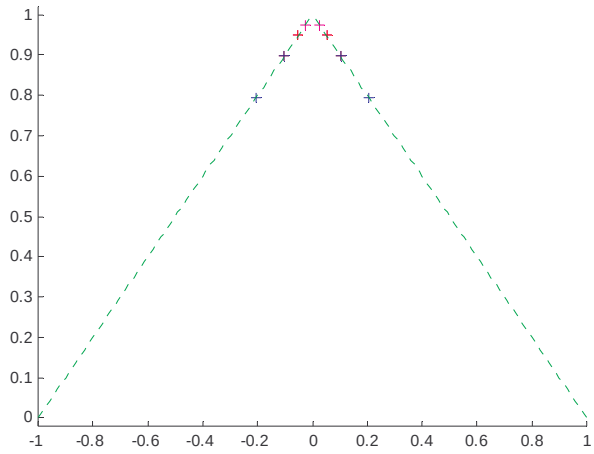

Figure 10: *Possible ΔΔ tracking pairs with 3rd SW version.n*

VII. OBSERVATION OF CORRELATION FUNCTIONS

One of the tasks of the test plan is to observe the correlation function of the signal affected by the evil waveform with the local C/A code. That analysis is done to determine what exactly is the real influence of evil waveforms on true receivers, and also to check how close the correlation shapes predicted with the simulation software used for SARPS validation are to the observed functions.

Figure 11 shows the observed correlation function together with the predicted correlation function for a model A evil waveform (delta=0.12):

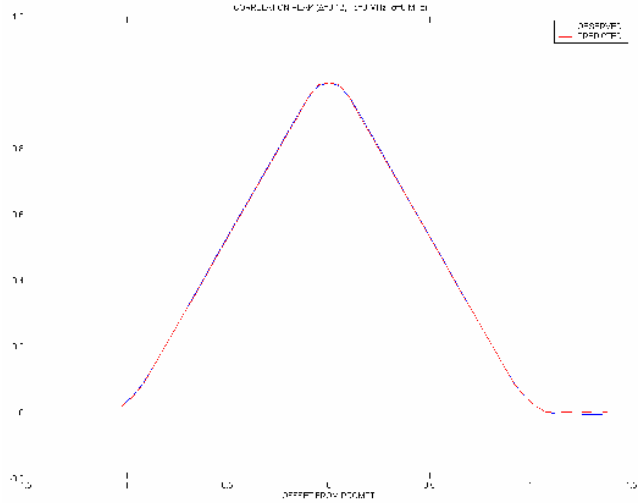

Figure 11 : *Model A (Δ=0.12 Tc) Predicted and Observed Correlation function.*

As we can by comparing figures 7 and 11 and following section III, that function has a plateau at its top, rounded by the receiver IF filter.

Figure 12 shows the deviation between the observed and the predicted correlation function for that model A evil waveform (delta=0.12).

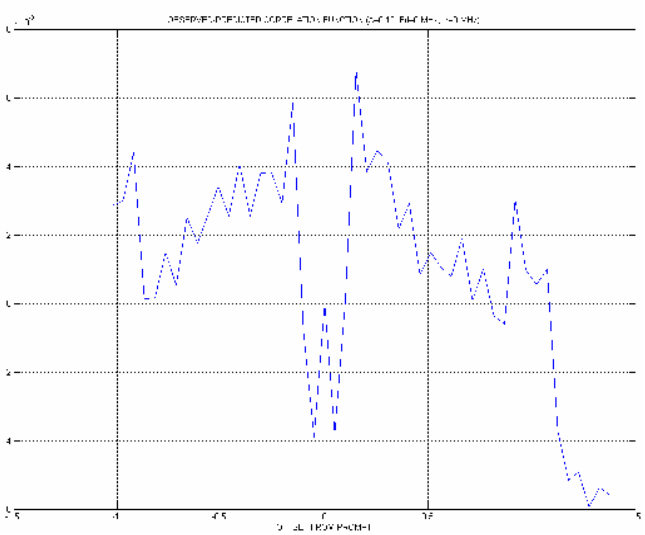

Figure 12: *Difference between observed and predicted model A correlation functions*

The largest prediction error has a value of 0.004, which is very small. The shape of the observed model A autocorrelation function is remarkably close to the theoretical shape.

Figure 13 presents the comparison of observed and predicted correlation functions for a model B evil waveform (Fd=4 MHz, sigma=0.8):

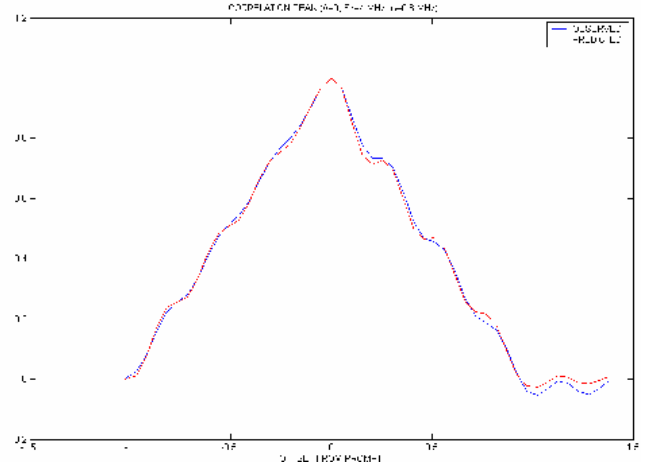

Figure 13: *Comparison of observed and predicted model B correlation function*

Figure 14 shows the deviation between the observed and the predicted correlation function for that model B evil waveform model B evil waveform (Fd=4 MHz, sigma=0.8).

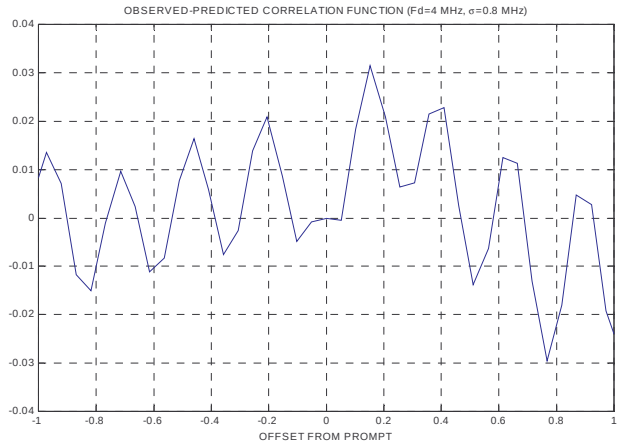

Figure 14: Difference between observed and predicted model B correlation functions

As we can see from these 2 figures, the main effect of the oscillations is predicted with good accuracy although a deviation is visible.

Globally, that deviation has a maximum value of 0.05, and is globally lower than 5% in the interval [-0.5; 0.5] chip of the correlation function.

We can note however here that the deviations on the horizontal axis may induce differences when predicting the tracking errors because of the asymmetrical differences between the left and the right side of the function. That point will be developed later when discussing the tracking errors.

VIII. CODE TRACKING ERROR

Another task included in the test plan is to observe the tracking error induced by evil waveforms. That analysis is done to determine what exactly is the influence of evil waveforms on a receiver tracking loop and to compare the predicted values with the observed values.

Figures 15 and 16 show the evolution of the observed and predicted tracking errors induced by a model A evil waveform on an E-L 0.05 chip DLL and a 0.2 chip DLL.

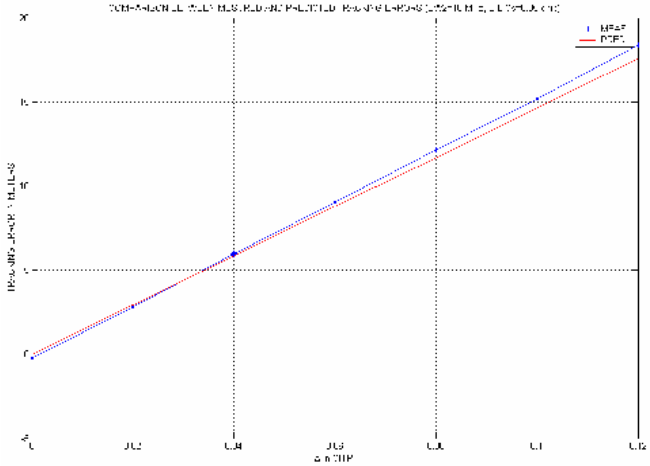

Figure 15 *: Comparison between observed and predicted effect of model A EWF on an E-L 0.05 chip DLL.*

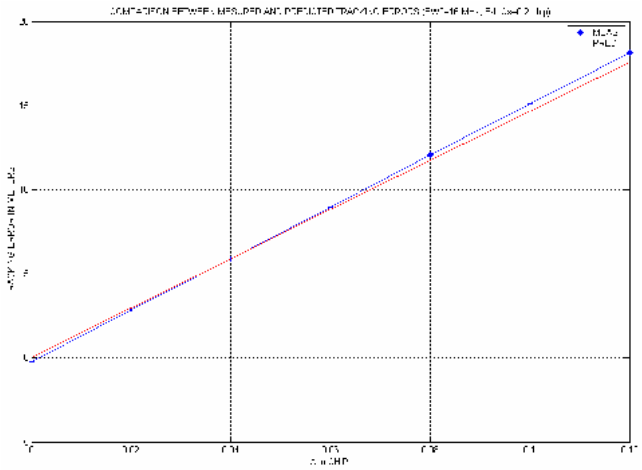

Figure 16 *: Comparison between observed and predicted effect of model A EWF on an E-L 0.2 chip DLL.*

Figure 17 represents the deviation between measured and predicted tracking errors for the different values of Δ for a double-delta DLL (Cs=0.05-0.1 Tc):

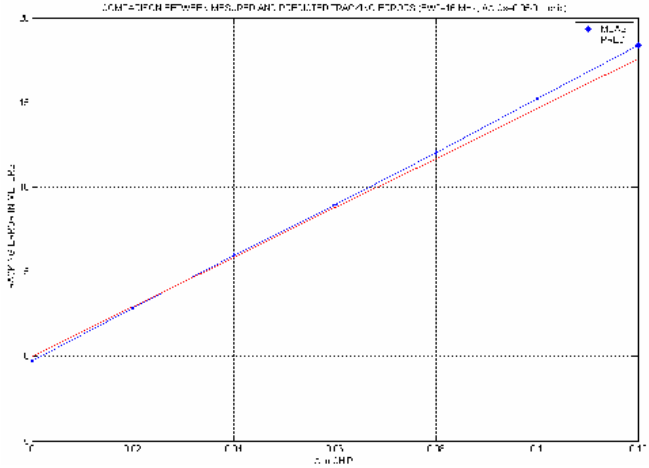

Figure 17*: Comparison between measured and predicted Model A errors (Cs=0.05-0.1 Tc)*

The linear evolution of the tracking error seen on these 2 figures can be explained by the predicted effect of a model A evil waveform on the correlation peak as seen in section III. In the case of an infinite bandwidth receiver, a model A evil waveform creates a plateau of width Δ on the correlation function and shifts the correlation function by Δ/2. Therefore, as the receiver used has a wide bandwidth (BW2=16 MHz), the tracking error grows as Δ/2 as long as Δ is lower than the chip spacing. Some distortions to that simple value are introduced when Δ is larger than the chip spacing.

The software used to predict the measurement error takes all this into account, but we can see that the predicted value deviates from the observed value as Δ grows (0.8 m for Δ=0.12 *Tc* for a 0.05 chip DLL in figure 15, 0.6 m for Δ=0.12 *Tc* for a 0.2 chip DLL in figure 16). That behaviour may be due to several factors: first of all, the Δ value affecting the PRN modulation may have a few percent incertitude. Secondly, as the DLL chip spacing is smaller than Δ, the DLL locks on a point that is difficult to predict because of the flatness of the discrimination function in those cases.

Globally, the error is lower than 0.8 m for all configurations tested and for model A EWF, which is satisfying.

Figure 18 represents the evolution of the observed tracking error as a function of F_d and σ. As we can see, for a specific σ, the error decreases when Fd increases. This is due to the combinations of two effects: first of all, as Fd increases, the tracking error decreases in the case of an infinite bandwidth receiver. Then, the filtering effect applied by the receiver front-end filter reduces the amount of high-frequency components entering the tracking loops. As we can see, the effect of model B evil waveforms is quite constant close to 0 starting from Fd=9 MHz.

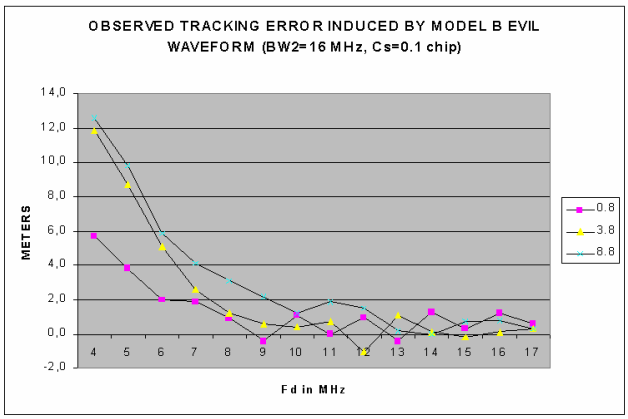

Figure 18: *Evolution of the observed tracking error in presence of a model B evil waveform (Cs=0.1 Tc).*

Figure 19 shows a comparison between the observed and predicted tracking errors induced by a model B evil waveform on an E-L 0.1 chip DLL.

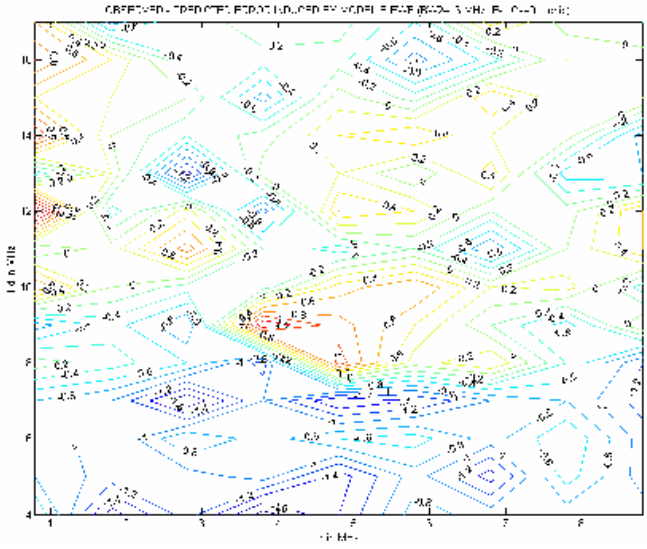

Figure 19: *Deviation between the observed and the predicted tracking error (model B evil waveform, Cs=0.1 Tc).*

As we can see in figure 19, the total average value of the prediction error is –0.2 m and the standard deviation is 0.6 m, which is globally a good result. However, those 2 figures do not reflect local disparities. Indeed, we can see that the deviation between the observed and predicted tracking errors is maximum when Fd is lower than 8 MHz. In that region, the largest deviation is –1.3 m (observed 6.2 m / predicted 7.5 m) for Fd=5 Mhz/σ=2.8 MHz and Fd=7 Mhz/σ=4.8 MHz. The average value of the prediction error for Fd ≤ 8 MHz is –0.4m with a standard deviation of 0.6 m, while the average value of the prediction error for Fd> 8 is 0 m with a standard deviation of 0.5 m.

One of the first ideas to explain the deviation in the lower frequency area (Fd ≤ 8 Mhz) is that this effect may be due to the implementation of the second order filter that was done on the FPGA. The waveform is encoded on 8 bits, which is perhaps too small a number of bits to represent the waveform, and the sampling frequency is 98.208 MHz while the sampling frequency used in the prediction software is 306.9 MHz,. However, we ran simulations taking into account these differences. The prediction error with these adaptations only changed by less than 20 cm.

We think that the large deviations between the observed and predicted measurement errors is related to a large deviation between the observed and predicted correlation function at its top (in the vicinity of the tracking correlator pair).

Figure 20 shows the observed and the predicted correlation function for delta =0, Fd=5, σ=2.8.

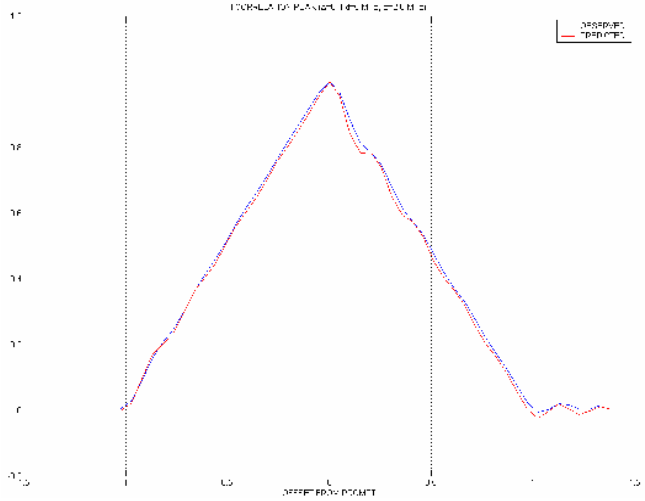

Figure 20 : *Observed and predicted model B correlation function (Fd=5, σ=2.8)*

Figure 21 shows the difference between the observed and the predicted correlation function for delta=0, Fd=5, sigma=2.8.

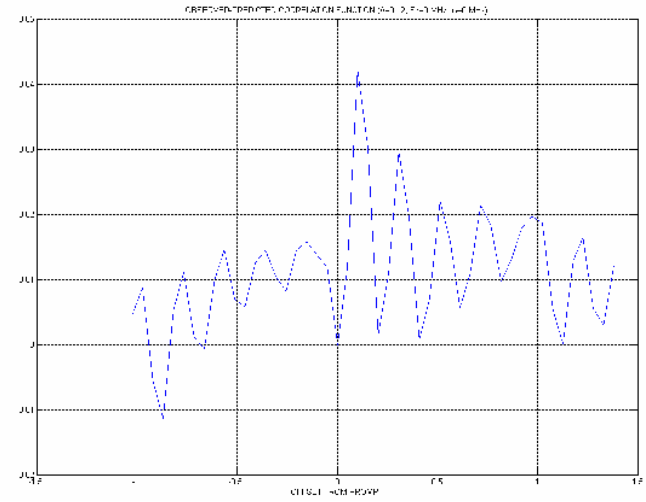

Figure 21: *Difference between observed and predicted model B correlation functions (delta=0, Fd=5, σ=2.8)*

The vertical error reaches 0.042 and we can see that the asymmetry on the horizontal axis is quite large (larger than what we saw for Fd=4, sigma=0.8 in section VII).

Figure 22 shows the observed and the predicted correlation function for delta=0, Fd=7, σ=4.8:

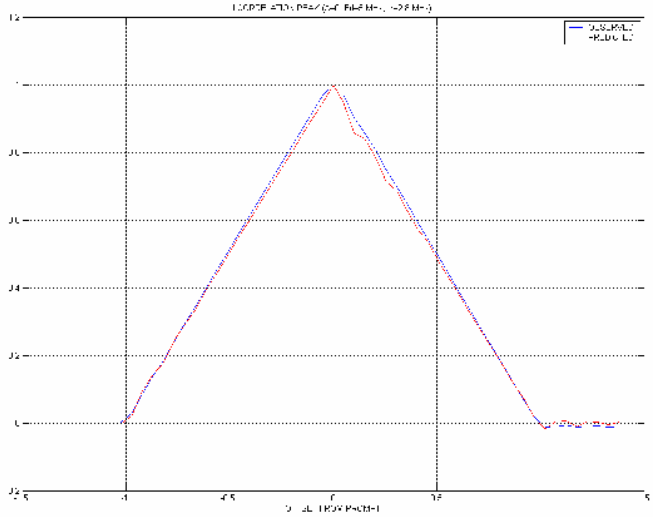

Figure 22 : *Observed and predicted model B correlation function (delta=0, Fd=7, σ=4.8)*

Figure 23 shows the difference between the observed and the predicted correlation function for delta=0, Fd=7, sigma=4.8.

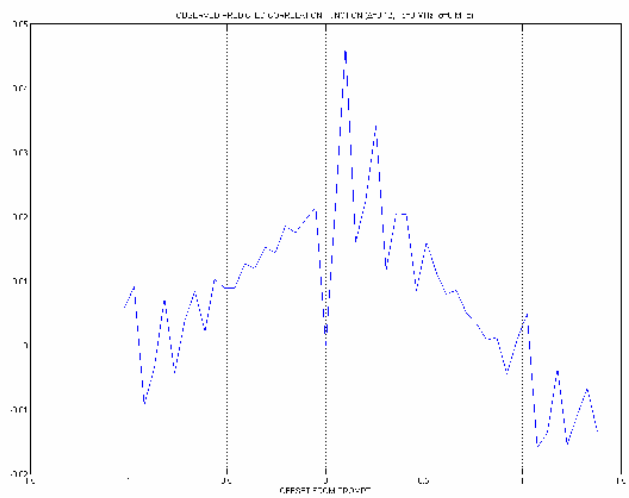

Figure 23: *Difference between observed and predicted model B correlation functions (delta=0, Fd=7, σ=4.8)*

The error reaches 0.0465 and we can see again that the asymmetry on the horizontal axis is quite large (larger than what we saw for Fd=4, sigma=0.8 in section VII).

Other DLLs tested for model B include E-L with Cs=0.2 and double-delta Cs=0.05-0.1.

For model B, Cs=0.2, the average value of the prediction error is 1.3 m, the standard deviation is 1.4 m and the max error is 4 m (Fd = 8 MHz, σ =2.8 MHz). Again, the error may be due to correlation function prediction error at 0.2 Tc

For model B, ΔΔ Cs=0.05-0.1, the average value of the prediction error is -4.7 m, the standard deviation is 2.4 m and the max error is -10.4 m (Fd = 4 MHz, σ = 0.8 MHz). In that case, we think the error may be due to wrong DLL model (MET vs double-delta).

For model C, we tested the values with a DLL Cs=0.1 Tc. The results are:

- Δ=0.02: Mean=-0.9 m, std=0.3 m, max=-1.3 m
- Δ=0.04: Mean=-0.8 m, std=0.5 m, max=-1.7 m
- Δ=0.06: Mean=-0.2 m, std=0.5 m, max=-1.4 m
- Δ=0.08: Mean=0.5 m, std=0.4 m, max=1.1 m
- Δ=0.10: Mean=2.4 m, std=0.6 m, max=3.6 m
- Δ=0.12: Mean=5.3 m, std=1.3 m, max=7.5 m

As we can see, the results are good up to Δ = 0.08 Tc. We think that the prediction error could be linked with correlation functions prediction error presented above (asymmetry).

IX. SQM PERFORMANCE

Finally, the last task has intended to implement and test performance of SQM techniques (version SQM 2b, [Macabiau and Chatre, 2000]) using the specific software version (4 channels with 12 correlators each) presented in section VI.

The SQM implemented is SQM2b [Macabiau and Chatre, 2000], where 11 test metrics are computed from the provided correlator outputs. These 11 test metrics are all formed using the 3 generic expressions:

$$\Delta_{\pm d} = \frac{I_{-d} - I_{+d}}{2I_P},\ R_{\pm d} = \frac{I_{-d} + I_{+d}}{2I_p}, R_d = \frac{I_d}{I_p}$$

where

- I_d is the correlator output on the I channel with offset d from the prompt
- I_P is the prompt correlator output on the I channel

The 11 test metrics used are:

(1) $R_{\pm 0.075}$, (2) $R_{-0.075}$, (3) $R_{+0.075}$, (4) $\Delta_{\pm 0.075}$- $\Delta_{\pm 0.05}$, (5) $R_{-0.05}$, (6) $R_{+0.05}$,(7) $\Delta_{\pm 0.1}$- $\Delta_{\pm 0.05}$, (8) $R_{-0.1}$, (9) $R_{+0.1}$, (10) $R_{\pm 0.05}$, (11) $R_{\pm 0.1}$

The implemented thresholds have been those published in [Macabiau and Chatre, 2000].

The predicted SQM 2b performance for Model B evil waveform is shown in table 1, where "1" means the evil waveform is detected:

Fd\Sigma	0.8	1.8	2.8	3.8	4.8	5.8	6.8	7.8	8.8
4	1	1	1	1	1	1	1	1	1
5	1	1	1	1	1	1	1	1	1
6	1	1	1	1	1	1	1	1	1
7	1	1	1	1	1	1	1	1	1
8	1	1	1	1	1	1	1	1	1
9	1	1	1	1	1	1	1	1	1
10	1	1	1	1	1	1	1	1	1
11	1	1	1	1	1	1	1	1	1
12	1	1	1	1	1	1	1	1	1
13	1	1	1	1	1	1	1	1	1
14	1	1	1	1	1	1	1	1	1
15	0	0	0	0	0	0	0	0	0
16	0	0	0	0	0	0	0	0	0
17	0	0	0	0	0	0	0	0	0

Table 1: *Predicted SQM 2b performance on model B.*

Table 2 shows the observed SQM performance for model B.

Fd\Sigma	0.8	1.8	2.8	3.8	4.8	5.8	6.8	7.8	8.8
4	1		1		1		1		1
5	1		1		1		1		1
6	1		1		1		1		1
7	1		1		1		1		1
8	1		1		1		1		1
9	1		1		1		1		1
10	1		1		1		1		1
11	1		1		1		0		0
12	1		0		0		0		0
13	0		0		0		0		0
14	1		0		0		1		0
15	0		0		0		0		0
16	1		0		0		0		0
17	1		0		0		0		0

Table 2: *Measured SQM 2b performance on Model B (grayed cells were were not tested).*

As we can see, the shape of the observed detection volume is very close to the shape of the predicted performance, except that:

- The upper Fd limit below which one all Evil Waveform are detected is Fd=10 MHz instead of the predicted Fd=14 MHz,

- The detection shape is triangular for Fd=11 MHz and Fd=12 MHz,.
- Some strange detection points appear: (Fd=14, σ =0.8), (Fd=16, σ =0.8), (Fd=17, σ =0.8), (Fd=14, σ =6.8).

The fact that the SQM is failing to detect evil waveforms for lower *Fd* than predicted can be explained by the inadequacy between the 16 MHz IF filter model used for predictions and the true filter used in the receiver, especially concerning the group delay variations with frequency.

The triangular shape of the detection volume, as well as the strange detection points appearing may be due to the reality of the 2nd order filter implementation in the EWF generation board.

Table 3 shows the predicted SQM performance on model B Evil Waveform when the IF filter is modeled as an 8th order Butterworth filter. We see again the triangular shape very close to the observed detection volume shown in table 2. Note that this filter model is adequate here, but is inadequate for the prediction of the range measurements.

Fd\Sigma	0.8	1.8	2.8	3.8	4.8	5.8	6.8	7.8	8.8
4	1	1	1	1	1	1	1	1	1
5	1	1	1	1	1	1	1	1	1
6	1	1	1	1	1	1	1	1	1
7	1	1	1	1	1	1	1	1	1
8	1	1	1	1	1	1	1	1	1
9	1	1	1	1	1	1	1	1	1
10	1	1	1	1	1	1	1	1	1
11	1	1	1	1	1	1	1	1	1
12	1	1	1	1	1	1	0	0	0
13	1	1	0	0	0	0	0	0	0
14	0	0	0	0	0	0	0	0	0
15	0	0	0	0	0	0	0	0	0
16	0	0	0	0	0	0	0	0	0
17	0	0	0	0	0	0	0	0	0

Table 3: *Predicted SQM 2b performance with 8th order Butterworth filter.*

Finally, table 4 shows the predicted performance for model C Evil Waveforms:

Delta	Fd/Sigma	0.8	1.8	2.8	3.8	4.8	5.8	6.8	7.8	8.8
0,04	7	1	1	1	1	1	1	1	1	1
	8	1	1	1	1	1	1	1	1	1
	9	1	1	1	1	1	1	1	1	0
	10	0	0	0	0	0	0	0	0	0
	11	0	0	0	0	0	0	0	0	0
	12	0	0	0	0	0	0	0	0	0
	13	0	0	0	0	0	0	0	0	0
0,08	7	1	1	1	1	1	1	1	1	1
	8	1	1	1	1	1	1	1	1	1
	9	1	1	1	1	1	1	1	1	1
	10	1	1	1	1	1	1	1	1	1
	11	1	1	1	1	1	1	1	1	1
	12	1	1	1	1	1	1	1	1	1
	13	1	1	1	1	1	1	1	1	1

Table 4: *Predicted SQM 2b performance on Model C.*

The following table shows the observed performance for some relevant parameters of model C Evil Waveforms:

Delta	Fd/Sigma	0.8	1.8	2.8	3.8	4.8	5.8	6.8	7.8	8.8
0,04	7	1		1		1		1		1
	8	1		1		1		1		1
	9	0		1		1		0		0
	10	0		0		0		0		0
	11	0		0		0		0		0
	12	0		0		0		0		0
	13	0		0		0		0		0
0,08	7	1		1		1		1		1
	8	1		1		1		1		1
	9									
	10	1								1
	11									
	12									
	13	1								1

Table 5: *Measured SQM 2b performance on Model C.*

Again, as we can see, the observed performance is very close to the predicted performance: the only difference appears for Δ=0.04, Fd=9 MHz, and σ=0.8, σ=6.8, σ=8.8 MHz, which may be due to any of the two reasons already invoked: inadequacy of IF filter model, real implementation of 2nd order filter.

We finally made first assessments of the false alert rate of the SQM on live signals. The receiver is now connected to a real antenna located on the roof of the ENAC electronics department building. The antenna is a Novatel 600 pin wheel antenna. The thresholds used are the operational thresholds given in [Macabiau and Chatre, 2000]. Figures 24 and 25 show examples of evolution of the false alarm rate as a function of the elevation angle. The false alarm rate is globally around 15 %, which is far more than the targeted design rate, especially when the elevation angle is low.

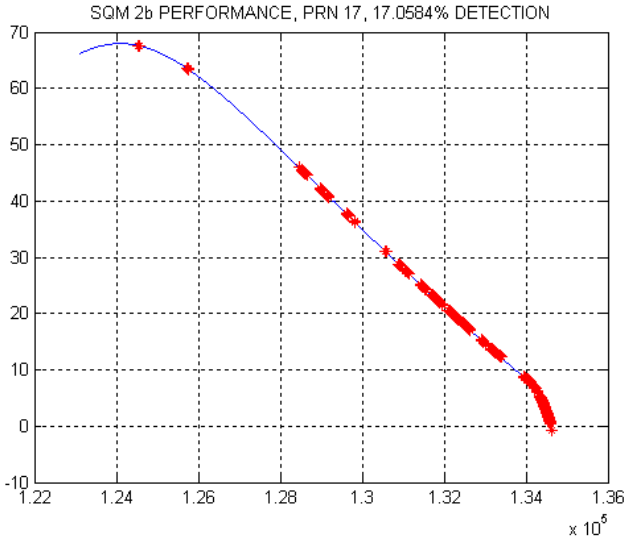

Figure 25 : *Observed SQM false alarm rate as a function of elevation angle (thresholds = simulation thresholds used for SARPS validation).*

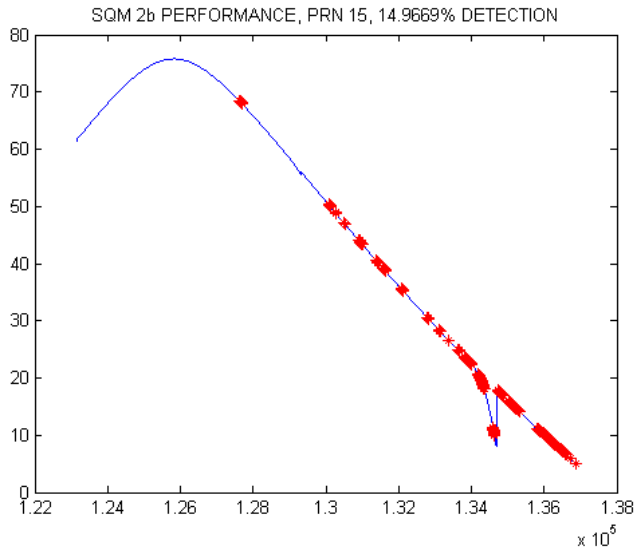

Figure 26 : *Observed SQM false alarm rate as a function of elevation angle (thresholds = simulation thresholds used for SARPS validation).*

Achieving a false alarm rate lower than the target in this environment necessitates to inflate the thresholds. But it remains to determine now what would be the SQM performance with the adapted thresholds at this site.

Of course, the quality of the experimental site is questioned. That is why another work to be carried out is the evaluation of the SQM performance on live signals at the TLS airport. Indeed, that site is much cleaner that the ENAC site, and corresponds to the type of environment for which the SQM thresholds used for SARPS validation have been adopted.

X. CONCLUSION

A test-bed for evaluation of the effect of evil waveforms on real receivers has been developed for ESTEC. That test-bed is designed to provide knowledge on the true impact of evil waveforms on the correlation function and on the tracking error, as well as to test the performance of SQM techniques.

The test-bed is composed of a baseband generator that can generate all evil waveforms in models A, B and C, delivering a signal to a vector signal generator to which a real receiver can be connected for long test periods.

Correlation function observations show a good consistency between the predicted and observed deformations for all evil waveform types (less than 5% error in the [–0.5; 0.5] chip region.

The pseudorange error measurements in most of the possible cases have been done. The analyses of the observed and predicted errors that were conducted are satisfying for model A evil waveforms (0.8 m max deviation between observations and predictions). For model B evil waveforms, those analyses show that the prediction error is small for model B (max -1.4 m Cs=0.1, max 4 m Cs=0.2, max –10.4 ΔΔ Cs=0.05-0.1 but doubt about disc. function). For model C, the prediction error is small ($0 \le \Delta \le 0.08$: max –1.7m Cs=0.1, $0.1 \le \Delta \le 0.12$: max 7.5m Cs=0.1).

We can say that the quality of the predictions depends on the DLL discrimination function. We can also say that the heoretical predictions made with adaptation of the model to the generation board do not improve the quality of the results. Deviations may be due to unexpected / unmodeled behaviour of the receiver.

Tests of SQM performance using the EWF generator show a good consistency between predicted and observed behaviour, and reveal a mismatch between the actuel receiver IF filter and the modelled IF filter.

Tests of SQM performance on live signals using Novatel 600 antenna on building roof and thresholds used for SARPS validation show a very high false alarm rate (15 %) that would necessitate inflation of SQM thresholds particularly at low elevation angles. Such an inflation would degrade the SQM detection capability in presence of an EWF. This remains to be confirmed through the analysis of the SQM performance on live signals at TLS airport.

REFERENCES

[ENGE et al., 1999] P. ENGE, E. PHELTS and A. MITELMAN, « Detecting Anomalous Signals from GPS Satellites », Global Navigation Satellite System Panel meeting, Toulouse October 18-29 1999, working paper 19.

[MACABIAU and CHATRE, 2000] C. MACABIAU, E. CHATRE, « Signal Quality Monitoring for Protection of GBAS Users Against Evil Waveforms », ION GPS 2000.

[MACABIAU et al., 2001] C. MACABIAU, W. VIGNEAU, D. HOUZET, « Evil Waveform Test-Bed Design », Navitec-01, ESTEC.

[MITELMAN et al., 2000] A. MITELMAN, E. PHELTS, D. AKOS, S. PULLEN, P. ENGE, « A Real-Time Signal Quality Monitor for GPS Augmentation Systems », ION GPS 2000.

[PHELTS et al., 2000] E. PHELTS, A. MITELMAN, S. PULLEN, D. AKOS, P. ENGE, « Transient Performance Analysis of a Multicorrelator Signal Quality Monitor », ION GPS 2000.